Size-dependent persistent photocurrent and its origin in dc sputtered indium oxide films under UV and sub-band gap illuminations

Prabal Sen, M. Balasubrahmaniyam, Durgesh Kar, and S. Kasiviswanathan

Citation: Journal of Applied Physics **121**, 185303 (2017); doi: 10.1063/1.4983077
View online: http://dx.doi.org/10.1063/1.4983077
View Table of Contents: http://aip.scitation.org/toc/jap/121/18
Published by the American Institute of Physics

Size-dependent persistent photocurrent and its origin in dc sputtered indium oxide films under UV and sub-band gap illuminations

Prabal Sen, M. Balasubrahmaniyam,[a] Durgesh Kar, and S. Kasiviswanathan[b]
Department of Physics, Indian Institute of Technology Madras, Chennai 600 036, India

(Received 15 February 2017; accepted 24 April 2017; published online 10 May 2017)

The size and spectral dependence of the persistent photocurrent (PPC) of dc sputtered indium oxide (IO) films has been studied under UV and sub-band gap illuminations. PPC follows bi-exponential decay with a fast and a slow process having time constants (denoted by τ_f and τ_s, respectively) that differ by about two orders of magnitude. τ_s is associated with carrier scattering from an initial surface state to a surface or bulk state with the former dominating below a characteristic length scale of ~60 nm. On the other hand, τ_f is characterized by the process where both the initial and final states are surface related. Treating the IO film surface with tetramethyl tetraphenyl trisiloxane (TTTS) decreases τ_s by a factor of 5 with τ_f remaining almost unaffected, which is a clear indication of reduction of defects specific to the slow relaxation process. Based on the molecular structure and chemical activity of TTTS, it is suggested that TTTS may passivate mainly the dangling oxygen-bonds at the film surface. The spectral dependence of τ_s indicates that the associated surface states exhibit a maximum around 2.5 eV above the level from where strong optical transitions are allowed. *Published by AIP Publishing*. [http://dx.doi.org/10.1063/1.4983077]

I. INTRODUCTION

The photogenerated current that continues to decay after the removal of the excitation source is usually referred to as persistent photocurrent (PPC) when the relaxation time is of the order of 100 s or more.[1,2] It is one of the main parameters that influences the characteristics of optoelectronic detectors and gas sensors. The study of PPC attracts attention, especially in semiconducting metal oxides as they are widely used in gas sensing and UV detection. The origin of PPC in oxide semiconductors is usually traced to bulk or surface related defect states resulting from oxygen vacancies, interstitial defects, or adsorbed gas molecules on the surface.[3–10]

Indium oxide (IO) is one of the widely studied metal oxide semiconductors with a band gap of ~2.9 eV.[11,12] When doped with tin, IO exhibits about 90% transmittance in the visible region and a plasma edge at the near infrared region leading to high electrical conductivity. Denoted as ITO in this form, it is one of the widely used transparent electrodes in flat panel displays, solar cells, and other optoelectronic devices. It is also possible to vary the conductivity of IO films by several orders without an external dopant. In fact, off-stoichiometric IO has been considered as a back transparent electrode for organic light emitting diodes. The other applications envisaged include IO based thin film transistors and all transparent p-n junctions. The principal application of IO, however, is in the field of gas sensing, as a conductance-based solid state gas transducer. IO has been found to exhibit good sensitivity to inflammable gasses such as H_2, CH_4, and other hydrocarbons[13–15] and air pollutant gases such as CO, NH_3, and NO_2.[13,16–20] Additionally, being a wide gap semiconductor, IO is also being studied for UV and ozone sensing.[21–23] Although UV sensing is based on transitions near the fundamental gap, gas sensing relies on the existence of mainly surface defects. Gas molecules can adhere to the defects through physisorption or chemisorption, resulting in change in conductance, an easily measurable parameter. The gas sensing properties of semiconducting metal oxides are governed primarily by the surface defects which give rise to deep or shallow surface states in the gap.[26–28] On the other hand, these surface states, which actually aid gas sensing, may act as carrier traps leading to PPC that can interfere with the sensing mechanism. Also, PPC is the major hurdle in using IO as the UV detector. Although carrier generation takes place on a fast time scale, carrier relaxation proceeds through intermediate trap states, stretching the response time.[23] Although PPC is mainly associated with trap states, it can also result from space charge layers.[1,2,24,25] Charges accumulated at the interfaces[24,25] or Fermi level pinning due to surface defects can cause band bending at the interface or surface,[1,2] which will result in spatial separation of electrons and holes and hence PPC with large decay constants.

PPC in general is governed by exponential or stretched exponential decay, depending on the functional form of the decay constant. The stretched exponential form results when the decay constant has power law dependence on time. Several reports are available on the photoresponse of IO films under above-band-gap (UV) illumination.[23,29–32] PPC in IO was first observed in the study of photoredox reaction under UV illumination-ozone exposure cycles.[21,29,30,33–36] When the IO films were exposed to UV followed by ozone exposure, the conductivity changed by several orders of magnitude with a time constant of several minutes.[21,29,36] The primary observation was that all changes are confined to the surface of the films. A recent study of PPC in highly crystalline RF-sputtered IO films showed PPC decay to be

[a]Present address: Tata Institute of Fundamental Research, 1, Homi Bhabha Road, Mumbai 400 005, India
[b]Electronic mail: kasi@iitm.ac.in

governed by a stretched exponential with a time constant of about 10 h which is quite large.[23] Brinzari *et al*. studied the spectral dependence of photoredox characteristics of nanocrystalline IO films grown by spray pyrolysis.[37] They used the ac method and observed non-zero photoresponse under sub-band gap (SBG) illumination with a peak around 2.9 eV. Thin films formed by spin-coating polyvinyl-alcohol treated and untreated IO nanoparticles dispersed in ethanol were studied for UV sensing.[32] The response time has been found to decrease by a factor of 2 due to PVA treatment.[32] The photoresponse of thin films of IO nanorods, synthesized by the vapor-liquid-solid growth process was studied under 405 nm illumination.[38] The decay of PPC was found to be bi-exponential with a slow and a fast time constants of 35 s and 250 s, respectively.[38]

The previous discussion shows that most of the studies on PPC are confined to UV irradiation and the PPC decays with large time constants. The aim of the present work is to probe the thickness and spectral dependence of PPC in IO thin films under UV and SBG illuminations and find if the decay constants can be reduced by suitable surface treatment. The results show that PPC follows a bi-exponential decay with a fast and a slow relaxation time. The thickness dependence of PPC is attributed to the scattering of charge carriers from surface states to bulk states as the density of bulk states increase with thickness. A significant reduction in the slow relaxation time is observed in films treated with a silicone, tetramethyl tetraphenyl trisiloxane (TTTS), which indicates the passivation of surface defects specific to the slow relaxation process.

II. EXPERIMENTAL DETAILS

Polycrystalline IO thin films of different thicknesses were grown on 1 mm thick 7059 Corning glass substrates by reactive dc-sputtering of indium target (purity ~99.99%) at an oxygen (99.99% pure) pressure of ~0.06 mbar with a base pressure of $\sim 10^{-6}$ mbar. In order to improve the crystalline quality, the as-deposited films were annealed in an oxygen atmosphere at 400 °C for 2 h. PPC measurements were made on films having different thicknesses, 24, 35, 70, 133, and 245 nm. Fig. 1 shows the optical transmittance

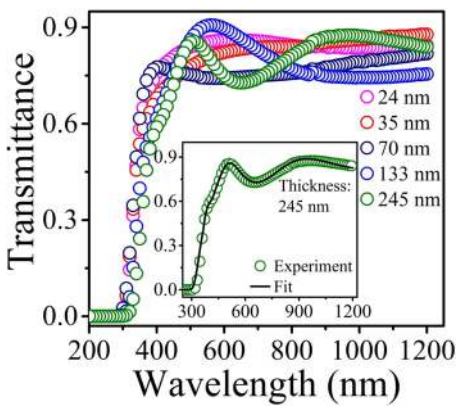

FIG. 1. Optical transmittance spectra of IO films with different thicknesses (24 nm–245 nm). The inset shows transmittance spectra together with theoretical fit (continuous line through data points) for a 245 nm thick film.

spectra of IO films with different thicknesses in the wavelength range of 200–1200 nm. The films are transparent with an average transmittance of about 80%. The oscillations in the transmittance spectra, appeared for higher thicknesses (133 and 245 nm), are due to the Fabry–Pérot interference. Film thicknesses were extracted from a numerical fit, and the inset to Fig. 1 shows, as an example, the measured data (open circles) together with the fit (continuous line) for the film with the highest thickness (245 nm). The optical band gap found from the fit was in the range of 3.60–3.75 eV. For films with thicknesses less than 100 nm (24, 35, and 70 nm), the thicknesses were crosschecked using X-ray reflectivity. Glancing angle X-ray diffraction confirmed that films were polycrystalline with a preferred orientation along the (222) direction (data not shown). The wavelength of the UV source used was 260 nm. Four different light emitting diodes having wavelengths 410, 465, 515, and 635 nm were used as SBG excitation sources. The intensity of all SBG sources was kept fixed at 50 mW/cm^2. The length and the width of each sample were 2.2 and 1.2 cm, respectively. Indium pads were used for electrical contacts and the Ohmic nature was verified by I–V measurements. The rise and decay of the photocurrent were measured using the Keithley 485 Autoranging Picoammeter keeping the sample bias constant at 5 V. After each measurement, the samples were kept in a dark chamber for about three weeks so that the initial resistance is recovered before the next measurement. All measurements were performed at room temperature in high vacuum ($\sim 10^{-5}$ mbar) primarily to avoid the influence of humidity.

III. RESULTS AND ANALYSIS

A. Persistent photocurrent

Fig. 2(a) displays the thickness dependence of change in PPC, ΔI ($=I(t)-I_{dark}$, where $I(t)$ and I_{dark} are the current at time t after illumination and the dark current, respectively) of IO films for the excitation wavelength of 410 nm. The increase in photocurrent during photoexcitation and its decay after the termination of excitation can be clearly seen in Fig. 2(a). The vertical dashed line separates the rise and decay of the photoresponse. The films exhibit similar variation of photocurrent with time when excited using other wavelengths (260, 465, 515, and 635 nm) as well. Although photoresponse under sub-band gap illumination is a clear indication of trap levels, the absorption due to the trap levels is not observed in the transmittance (Fig. 1). This is because the probability of trap to band transition is orders of magnitude smaller than that of the band-to-band transition. For the analysis, the decay profile is preferred since during decay there is no carrier generation as the excitation source is switched off. Fig. 2(b) shows the decay profile of ΔI, normalized with respect to its maximum value ΔI_{max} ($=I_{max}-I_{dark}$) for 410 nm excitation. Here, I_{max} is the value of photocurrent just before the illumination is switched off. In general, PPC has been shown to exhibit a different behavior depending on the nature of the governing physical mechanism.[3,23,38] The expressions which are mainly used to fit the PPC decay are single or bi-exponential, stretched exponential, and logarithmic in nature. We find that a bi-exponential expression

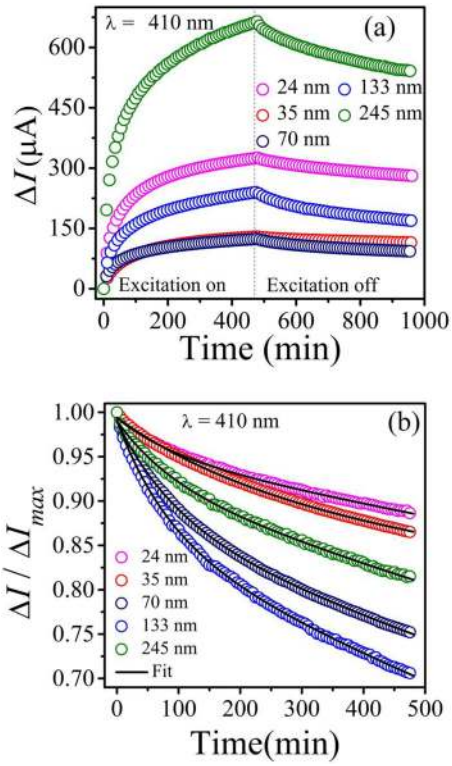

FIG. 2. (a) Change in photocurrent (ΔI) with time under 410 nm illumination for IO films with different thicknesses. The excitation source is switched off after 8 h of illumination. (b) Decay of normalized photocurrent ($\Delta I/\Delta I_{max}$) for IO films with different thicknesses (24 nm–245 nm) under 410 nm illumination.

(Eq. (1)) with a slow and fast relaxation time fits the decay profile well

$$\frac{\Delta I}{\Delta I_{\max}} = A_s \exp\left(-\frac{t}{\tau_s}\right) + A_f \exp\left(-\frac{t}{\tau_f}\right), \qquad (1)$$

where τ_s (τ_f) is the time constant associated with the slow (fast) mechanism. A_s and A_f are, respectively, pre-exponential factors for the slow and the fast decays. The solid lines through the data points in Fig. 2(b) show the fit using Eq. (1). τ_s and τ_f for films with different thicknesses are extracted from these fits for five different wavelengths, although the plot for only one wavelength (410 nm) is shown in Fig. 2(b). Similar bi-exponential response has been observed earlier in wide band gap semiconductors.[3,5] It has been shown that the slow time constant is predominantly due to the recombination in surface states, whereas the fast process is associated with bulk states[3–5,39] though the opposite has also been claimed.[40–42]

B. Thickness dependence of relaxation time

Fig. 3 shows the thickness dependence of τ_s for different photoexcitations. As the thickness increases, the value of τ_s decreases sharply. For instance, when the excitation wavelength is 465 nm, τ_s falls from $\sim 12 \times 10^3$ min (film thickness, 24 nm) to a minimum value of $\sim 2 \times 10^3$ min (film thickness, 133 nm). The trend is similar for all the excitation sources used, although the magnitude of the change differs.

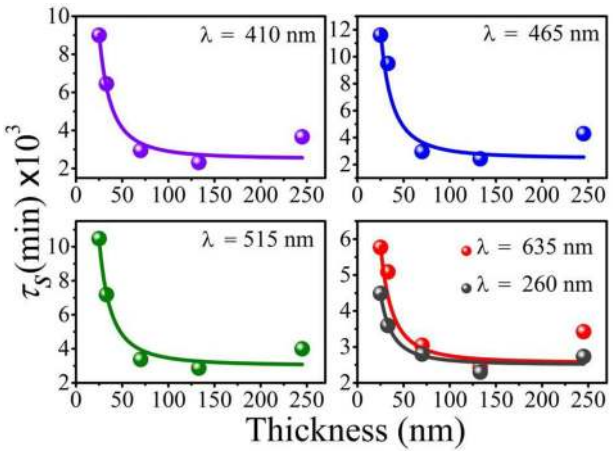

FIG. 3. Thickness dependence of τ_s of IO films for different excitation wavelengths (260, 410, 465, 515, and 635 nm). Continuous lines are polynomial fit using Eq. (3).

Continuous lines through the data points are fits from which length scales are extracted as discussed in the later sections in detail. Fig. 4(a) displays the thickness dependence of τ_f, obtained from the fit using Eq. (1) for different excitation wavelengths. Interestingly, unlike τ_s, τ_f does not show a systematic variation and is independent of thickness. For instance, the value of τ_f is ~50 min for all thicknesses, when the excitation wavelength is 515 nm. The pre-exponential factors, A_s and A_f, signify, respectively, the contributions of the slow and fast relaxation processes to the observed decay profile of PPC. Therefore, the ratio, A_s/A_f, is a measure of the relative strength of slow process with respect to the fast one. Fig. 4(b) shows the variation of A_s/A_f with film thickness for different excitation wavelengths. The relative strength of slow process decreases with thickness for all the excitations used, and the variation is quite similar to that exhibited by τ_s. To summarize, both τ_s and A_s/A_f are

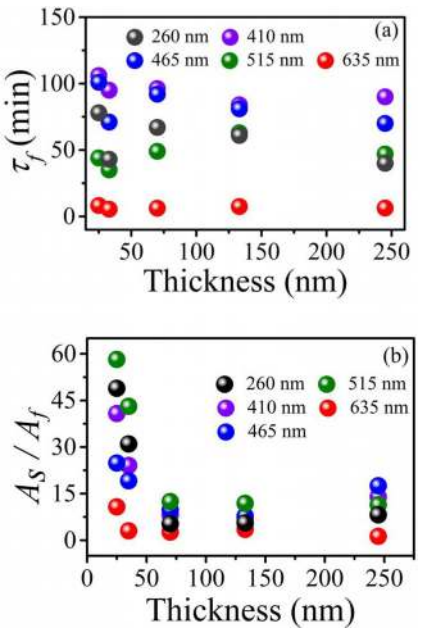

FIG. 4. (a) τ_f vs. thickness and (b) A_s/A_f vs. thickness for different excitation wavelengths (260, 410, 465, 515, and 635 nm).

strongly affected by thickness, whereas τ_f remains unaffected for all wavelengths. This clearly indicates that surface and bulk defect states contribute to τ_s and A_s/A_f, whereas τ_f may be associated with surface defect states alone.

High persistency is a result of trapping of photogenerated carriers at the defect states and the consequent slowing down of the recombination rate. In the present case, as the film thickness decreases, the persistency in the photocurrent increases and as we have seen the primary contributing factor is τ_s. The decrease in τ_s with thickness may be understood in the following way. The charge carriers at the surface can undergo two kinds of scattering: from an initial surface state to another surface state and from an initial surface state to a bulk state.[43] The scattering can involve emission or absorption of a phonon to ensure momentum conservation.[43] Therefore, τ_s is effectively the result of two different kinds of surface scattering, with the initial state always being a surface state and the final state being either a surface state or a bulk state. Under this assumption, τ_s can be written as

$$\frac{1}{\tau_s} = \frac{1}{\tau_{s\to s}} + \frac{1}{\tau_{s\to b}}, \tag{2}$$

where $\tau_{s\to s}$ and $\tau_{s\to b}$ represent, respectively, the relaxation time associated with the surface state to surface state scattering and the surface state to bulk state scattering. The scattering probability is given by the inverse of the relaxation time. As the film thickness decreases, the density of the available bulk states decreases. Consequently, the carrier-scattering probability from the surface states to bulk states decreases, which in turn increases τ_s. This observation is also corroborated by the variation of A_s/A_f with thickness (Fig. 4(b)). As the film thickness decreases, A_s/A_f increases, confirming that there is a relative increase in the contribution of a slow relaxation process to PPC. On the other hand, τ_f does not show clear thickness dependence that may be taken to indicate that it is associated with scattering of carriers from surface to surface states.

1. Characteristic length scale

Previous discussions have shown that the surface plays a crucial role in determining the decay of PPC. It is of interest to determine a length scale, which can help mark the thickness, below which $\tau_{s\to s}$ dominates. One way to extract the length scale is to fit the data to a polynomial in even powers of inverse length, which is given by the following equation:

$$\tau_s = C_0 + C_1\left(\frac{x_c}{x}\right)^2 + C_2\left(\frac{x_c}{x}\right)^4. \tag{3}$$

Here, x_c is the length scale and C_0, C_1, and C_2 are constants with appropriate dimension. The choice of even powers ensures that the variation is monotonic. In the limit $x \to \infty$, τ_s will have contribution solely from surface-to-bulk state scattering, whereas in the opposite limit $x \to 0$, the surface-to-surface state scattering will determine τ_s. Therefore, x_c will determine the crossover length. In Fig. 3, the continuous lines drawn through the data points are the fit using Eq. (3), which clearly reproduces the data well for all the wavelengths. The values of x_c for different wavelengths, obtained from the fit, are in the range of 55 to 61 nm, which shows that surface to surface state scattering dominates below about 60 nm. It may be noted from Fig. 3 that although the fit using Eq. (3) reproduces the data well at lower thicknesses, it underestimates τ_s for the 245 nm thick film for all the illumination wavelengths used. We believe that this may be due to the surface states induced surface band bending, which will become prominent as the thickness increases. Both generation and transport of carriers govern the photoresponse and since the built-in field acts in the opposite direction for the holes and electrons, they will be spatially separated. Consequently, the probability for recombination will be reduced, leading to delay in the carrier recombination. It is also to be noted here that surface band bending will be significant during the decay, as photo-induced carrier generation will greatly suppress the band bending during illumination. A recent study on PPC in GaN nanowires[1,2] has shown, apart from trap levels, surface band bending as the principal reason for PPC. Space charge controlled PPC has also been observed[25] more recently on Pentacene based organic thin film transistors.

C. Effect of surface passivation

Since the surface presents a discontinuity of the bulk, there is a large density of partially bonded indium and oxygen atoms at the surface. This gives rise to high density of surface states within the band gap. Further, IO is known to possess specific defects such as vacancies or interstitials of indium or oxygen.[44,45] These defects may be associated with the surface or bulk or both. Although it is difficult to control the bulk defects using post-processing treatments, surface defects can be reduced by using surface chemical passivation methods. In addition, through a careful choice of passivating agent, it is possible to reduce the defects selectively. Further, the results presented in Secs. III A and III B have suggested that surface defect states are mainly responsible for the PPC, and therefore, any change in the surface condition will affect both τ_s and τ_f. Since the present study is concerned with the photocurrent measurements, the passivating agent must be transparent in the visible region, to avoid any unintentional absorption of the incident radiation. In this context, we have used TTTS, a silicone with linear chemical formula $[CH_3Si(C_6H_5)_2O]_2Si(CH_3)_2$. It is dispersionless in the visible region with a refractive index of 1.56. Silicones, in general, have several active silane groups, which are well-known surface passivating agents[46,47] for metal oxides.[48,49] Recently, silicone treated ZnO nanoparticles have been found to exhibit large improvement in the anti-bacterial property[50,51] and also showed large enhancement in the photocurrent.[52]

Fig. 5 compares the decay of photocurrent of TTTS treated IO film with that of the untreated film. The film thickness is 133 nm and the measurements were carried out for all wavelengths. As seen from Fig. 5, there is a significant reduction in the persistency for the film treated with TTTS. In fact, τ_s is reduced by a factor of about five, and the magnitude of change in the value of τ_s is nearly the same for all wavelengths. Similarly, the ratio A_s/A_f, which is a measure

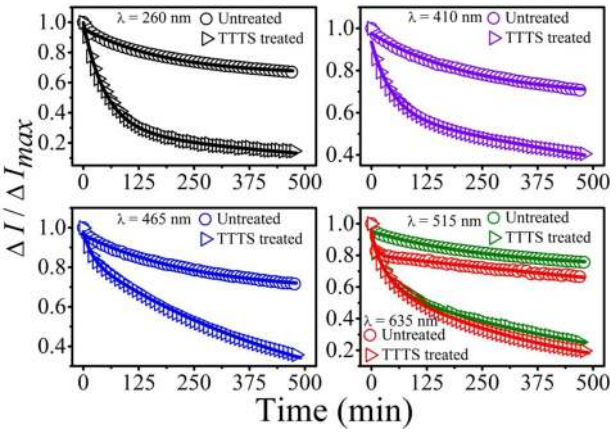

FIG. 5. Decay of normalized photocurrent ($\Delta I/\Delta I_{max}$) of TTTS treated and untreated IO films under different excitations. The thickness of the film is 133 nm. Continuous lines represent the bi-exponential fit.

of the relative strength of slow relaxation process with respect to the fast relaxation process, shows a large reduction. However, there is no significant and consistent change in the value of τ_f for all wavelengths. A comparison of the values of τ_s, τ_f, and A_s/A_f for untreated and TTTS treated IO film is presented in Table I. These observations clearly demonstrate that TTTS treatment reduces the surface defect states that are specific to the slow relaxation process, whereas the surface defects specific to the fast relaxation process remain unaffected. It is known that the adsorbed water molecules on the IO film surface can undergo photocatalytic splitting through the reactions, $H_2O + h^+ = OH + H^+$ and $OH + e^- = OH^-$, resulting in the generation of H^+ and OH^- ions.[37,53] As can be seen from Fig. 6, the molecular structure of TTTS has a siloxane (Si-O-Si) framework with organic side-chains. Siloxane can undergo hydrolysis in the presence of H^+/OH^- ions even at room temperature.[54,55] As a result of the hydrolytic cleavage of the Si-O-Si bond, silanol ($Si(CH_3)_2(OH)_2$) will form and also the silane groups will leave the TTTS silicone molecule.[47,54,55] The different surface defects that are known to contribute to defect states in IO include oxygen-dangling bonds resulting from oxygen enrichment or indium vacancies.[20,44] These dangling oxygen bonds can serve as nucleophilic groups and can coordinate to the silane groups, left from the TTTS molecule (Fig. 6). Since the unsaturated oxygen bonds on the IO surface get passivated, the density of surface defect states pertaining to oxygen dangling bonds will decrease. The reduction of the values τ_s and A_s/A_f indicates that defects related to oxygen dangling bonds are responsible for the slow relaxation

TABLE I. Comparison of τ_s, τ_f, and A_s/A_f values for untreated and TTTS treated IO film. The thickness of the film is 133 nm.

	State of the IO film									
Parameters	Untreated					Treated with TTTS				
Wavelength (nm)	260	410	465	515	635	260	410	465	515	635
τ_s (min) ($\times 10^3$)	2.30	2.32	2.43	2.87	2.43	0.57	0.80	0.59	0.66	0.37
τ_f(min)	61	83	80	63	10	49	55	60	48	12
A_s/A_f	5.56	6.80	7.82	11.8	3.50	0.44	2.50	0.19	1.36	0.43

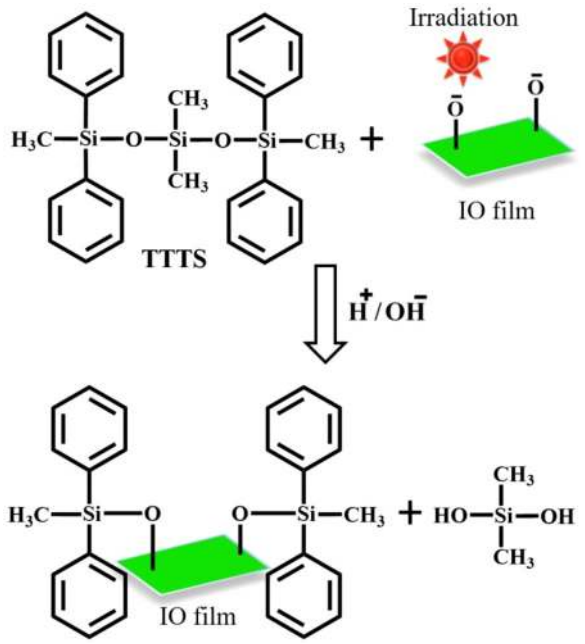

FIG. 6. Schematic representation of surface passivation of IO film through the chemical reaction with TTTS.

process. Thus, we can conclude that these observations, apart from substantiating our previous conclusion on the role of surface related defects in controlling PPC, have given insight into the possible origin of surface defect states and surface passivation of IO films by TTTS.

D. Spectral response of relaxation time τ_s

Spectral response of τ_s has been studied in order to understand the distribution of surface defect states. Fig. 7 shows the spectral responses of τ_s of IO films with different thicknesses. Since the decay time is proportional to the density of surface states, spectral dependence of τ_s should reflect the distribution of density of surface states that contribute to the slow relaxation process. Continuous lines through the data points represent the fit obtained by assuming Gaussian distribution of states as the density of surface or interface defect states are known to follow the Gaussian distribution.[25] Interestingly, spectral dependence of τ_s shows maximum

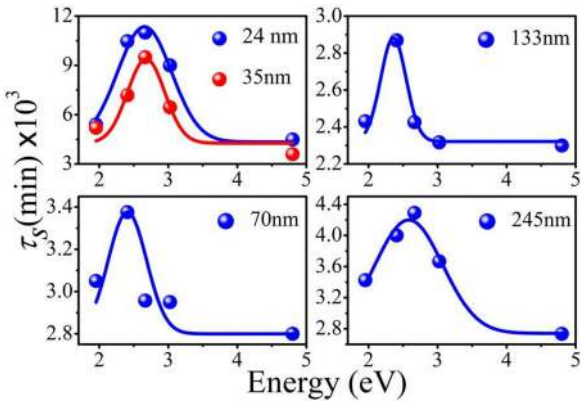

FIG. 7. Variation of τ_s with energy of the incident radiation for different film thicknesses. Continuous lines represent the Gaussian fit.

around 2.5 eV (Fig. 7) for all thicknesses. This in turn shows that the density of surface defect states that are associated with the slow relaxation process is distributed such that it is highest close to 2.5 eV, above the valence band. It is necessary at this point to discuss how the optical gap in IO is defined. Although it has been extensively reported that the band gap of IO is ~3.7 eV, recent studies have shown that the band gap is overestimated and is actually in the range of 2.7– 2.9 eV.[11,12] The calculations have shown that the transition from the valence band maximum (VBM) to the conduction band minimum is forbidden. The dominant allowed optical transition has been found to occur from levels ~0.8 eV below the VBM, which accounts for the large optical gap of ~3.7 eV.[11,12] As τ_s is found to be highest around the excitation energy of 2.5 eV, the density of surface defect states is maximum around 1.7 eV above the VBM or 2.5 eV above the level from where strong allowed optical transition can take place.

IV. CONCLUSIONS

We have measured the PPC of IO films under UV and SBG illuminations. The results show that PPC is governed by bi-exponential decay with a fast and a slow decay time constants, which differ by an order of 2. The thickness dependence of the decay constant associated with the slow process is attributed to the carrier scattering from the surface to bulk states. A surface length scale of about 60 nm has been estimated. The films treated with TTTS exhibit nearly 5-fold reduction in the slow decay constant, which is an interesting result from the viewpoint of UV sensing. From the spectral response of the slow relaxation time, we conclude that the density of surface states associated with the slow relaxation process is maximum around 2.5 eV above the level from where strong allowed optical transition is known to occur in IO films.

ACKNOWLEDGMENTS

This work was facilitated by Dr. J. S. Moodera, Francis Bitter National Magnet Laboratory, Massachusetts Institute of Technology, USA, and supported by Mr. S. Gopalakrishnan, Co-founder, Infosys Technologies, India, under Grant No. PHY/11-12/251/ALUM/SKAS. We also acknowledge Mr. Monojit Ghosal Chowdhury and Dr. Avik Kumar Pati of Department of Chemistry, IIT Madras, for their valuable contribution to the discussion.

[1]H. Chen, R. Chen, N. K. Rajan, F. Chang, L. Chen, K. Chen, Y. Yang, and M. A. Reed, Phys. Rev. B **84**, 205443 (2011).
[2]R. Calarco, M. Marso, T. Richter, A. I. Aykanat, R. Meijers, A. V. D. Hart, T. Stoica, and H. Luth, Nano. Lett. **5**, 981–984 (2005).
[3]J. Reemts and A. Kittel, J. Appl. Phys. **101**, 013709 (2007).
[4]P. Sharma, K. Sreenivas, and K. V. Rao, J. Appl. Phys. **93**, 3963 (2003).
[5]R. S. Aga, Jr., D. Jowhar, A. Ueda, Z. Pan, W. E. Collins, R. Mu, K. D. Singer, and J. Shen, Appl. Phys. Lett. **91**, 232108 (2007).
[6]F. Fang, D. X. Zhao, B. H. Li, Z. Z. Zhang, J. Y. Zhang, and D. Z. Shen, Appl. Phys. Lett. **93**, 233115 (2008).
[7]H. Kumar Yadav and V. Gupta, J. Appl. Phys. **111**, 102809 (2012).
[8]S. A. Studenkin, N. Golego, and M. Cocivera, J. Appl. Phys. **87**, 2413 (2000).
[9]S. P. Harvey, T. O. Mason, Y. Gassenbauer, R. Schafranek, and A. Klein, J. Phys. D: Appl. Phys. **39**, 3959 (2006).
[10]J. Nayak, J. Kasuya, A. Watanabe, and S. Nozaki, J. Phys.: Condens. Matter **20**, 195222 (2008).
[11]A. Walsh, J. L. F. Da Silva, S.-H. Wei, C. Körber, A. Klein, L. F. J. Piper, A. DeMasi, K. E. Smith, G. Panaccione, P. Torelli, D. J. Payne, A. Bourlange, and R. G. Egdell, Phys. Rev. Lett. **100**, 167402 (2008).
[12]O. Bierwagen, Semicond. Sci. Technol. **30**, 024001 (2015).
[13]H. Yamaura, J. Tamaki, K. Moriya, N. Miura, and N. Yamazoe, J. Electrochem. Soc. **143**, L36 (1996).
[14]V. Golovanov, M. A. Maki-Jaskari, T. T. Rantala, G. Korotcenkov, V. Brinzari, A. Cornet, and J. Morante, Sens. Actuator B **106**, 563 (2005).
[15]H. Yamaura, K. Moriya, N. Miura, and N. Yamazoe, Sens. Actuators B **65**, 39 (2000).
[16]V. Brinzari, G. Korotcenkov, M. Ivanov, V. Nehasil, V. Matolin, K. Masek, and M. Kamei, Surf. Sci. **601**, 5585 (2007).
[17]C. Cantalini, W. Wlodarski, H. T. Sun, M. Z. Atashbar, M. Passacantando, A. R. Phani, and S. Santucci, Thin Solid Films **350**, 276 (1999).
[18]H. Steffes, C. Imawan, F. Solzbacher, and E. Obermeier, Sens. Actuators B **78**, 106 (2001).
[19]V. Luhin, I. Zharsky, and P. Zhukowski, Acta Phys. Polonica A **123**(5), 837 (2013).
[20]V. Brinzari, B. K. Cho, and G. Korotcenkov, Appl. Surf. Sci. **390**, 897 (2016).
[21]G. Kiriakidis, M. Bender, N. Katsarakis, E. Gagaoudakis, E. Hourdakis, E. Douloufakis, and V. Cimalla, Phys. Status Solidi A **185**, 1, 27 (2001).
[22]C. Xirouchaki, G. Kiriakidis, T. F. Pedersen, and H. Fritzsche, J. Appl. Phys. **79**, 9349 (1996).
[23]A. Dixit, R. P. Panguluri, C. Sudakar, P. Kharel, P. Thapa, I. Avrutsky, R. Naik, G. Lawes, and B. Nadgorny, Appl. Phys. Lett. **94**, 252105 (2009).
[24]V. D. Mihailetchi, J. Wildeman, and P. W. M. Blom, Phys. Rev. Lett. **94**, 126602 (2005).
[25]S. Singh and Y. N. Mohapatra, J. Appl. Phys. **120**, 045501 (2016).
[26]S. Anantachaisilp, S. M. Smith, C. Ton-That, T. Osotchan, A. R. Moon, and M. R. Phillips, J. Phys. Chem. C **118**, 27150 (2014).
[27]M. J. S. Spencer, K. W. J. Wong, and I. Yarovsky, J. Phys.: Condens. Matter **24**, 305001 (2012).
[28]S. S. Kim, J. Y. Park, S.-W. Choi, H. S. Kim, H. G. Na, J. C. Yang, and H. W. Kim, Nanotechnology **21**, 415502 (2010).
[29]M. Bender, N. Katsarakis, E. Gagaoudakis, E. Hourdakis, E. Douloufakis, V. Cimalla, and G. Kiriakidis, J. Appl. Phys. **90**, 5382 (2001).
[30]N. Katsarakis, M. Bender, V. Cimalla, E. Gagaoudakis, and G. Kiriakidis, Sens. Actuators B **96**, 76 (2003).
[31]D. Zhang, C. Li, S. Han, X. Liu, T. Tang, W. Jin, and C. Zhou, Appl. Phys. A **77**, 163 (2003).
[32]D. Shao, L. Qin, and S. Sawyer, Proc. SPIE **8263**, 82630P (2012).
[33]M. Takeuchi, K. Inoue, S. Ozawa, and H. Nagasaka, Appl. Surf. Sci. **33/34**, 905 (1988).
[34]E. Gagaoudakis, M. Bender, E. Douloufakis, N. Katsarakis, E. Natsakou, V. Cimalla, and G. Kiriakidis, Sens. Actuators B **80**, 155 (2001).
[35]M. Himmerlich, A. Eisenhardt, T. Berthold, Ch. Y. Wang, V. Cimalla, O. Ambacher, and S. Krischok, Phys. Status Solidi A **213**(3), 831 (2016).
[36]H. Fritzsche, B. Pashmakov, and B. Claflin, Sol. Energy Mater. Sol. Cells **32**, 383 (1994).
[37]V. Brinzari, M. Ivanov, B. K. Cho, M. Kamei, and G. Korotcenkov, Sens. Actuators B **148**, 427 (2010).
[38]L. Qin, P. S. Dutta, and S. Sawyer, Semicond. Sci. Technol. **27**, 045005 (2012).
[39]Z. C. Feng, *Hand book of Zinc Oxide and Related Materials: Vol. Two, Devices and Nano-Engineering* (CRC Press, Taylor & Francis Group, Boca Raton, 2013), Vol. 2, p.153.
[40]Z. N. Urgessa, J. R. Botha, M. O. Eriksson, C. M. Mbulanga, S. R. Dobson, S. R. Tankio Djiokap, K. F. Karlsson, V. Khranovskyy, R. Yakimova, and P. Holtz, J. Appl. Phys. **116**, 123506 (2014).
[41]S. L. Chen, W. M. Chen, and I. A. Buyanova, Appl. Phys. Lett. **102**, 121103 (2013).
[42]Q. X. Zhao, L. L. Yang, M. Willander, B. E. Sernelius, and P. O. Holtz, J. Appl. Phys. **104**, 073526 (2008).
[43]A. V. Narlikar, *Frontiers in Magnetic Materials* (Springer, Berlin, 2005), pp. 306–307.
[44]P. Reunchan, X. Zhou, S. Limpijumnong, A. Janotti, and C. G. Van de Walle, Curr. Appl. Phys. **11**, S296 (2011).
[45]A. Walsh, Appl. Phys. Lett. **98**, 261910 (2011).

[46]D. Zhu, X. Nai, S. Lan, S. Bian, X. Liu, and W. Li, Appl. Surf. Sci. **390**, 25 (2016).
[47]H.-M. Tong, Y.-S. Lai, and C. P. Wong, *Advanced Flip Chip Packaging* (Springer, New York, 2013), pp. 176–177.
[48]K. Yabuki and A. Tofuku, U.S. patent 8,304,070 B2 (6 November 2012).
[49]K. Sakuta, U.S. patent 5,236,986 (17 August 1993).
[50]V. S. R. Rao and D. H. Gracias, U.S. patent 2004/0072436 A1 (15 April 2004).
[51]M. Hashimoto, K. Magara, and K. Nishida, European patent 2 781 486 A1 (24 September 2014).
[52]M.-S. Kim, J.-H. Han, D.-H. Lee, B.-H. O., S.-G. Lee, E.-H. Lee, and S.-G. Park, Microelectron. Eng. **97**, 130 (2012).
[53]A. Fujishima and K. Honda, Nature **238**, 37 (1972).
[54]S. L. Warring, D. A. Beattie, and A. James McQuillan, Langmuir **32**, 1568 (2016).
[55]M. Cypryk and Y. Apeloig, Organometallics **21**, 2165 (2002).